Coordination Chemistry Reviews 253 (2009) 2376–2386

Contents lists available at ScienceDirect

Coordination Chemistry Reviews

journal homepage: www.elsevier.com/locate/ccr

Review

Combining NMR spectroscopy and quantum chemistry as tools to quantify spin density distributions in molecular magnetic compounds

Martin Kaupp[a,*], Frank H. Köhler[b,*]

[a] Institut für Anorganische Chemie, Universität Würzburg, Am Hubland, D-97074 Würzburg, Germany
[b] Department Chemie, Technische Universität München, Lichtenbergstr. 4, D-85747 Garching, Germany

Contents

ARTICLE INFO

Article history:
Received 21 October 2008
Accepted 31 December 2008
Available online 10 January 2009

Keywords:
Magnetic materials
Spin density
NMR spectroscopy
Density functional theory
Paramagnetic NMR theory

ABSTRACT

NMR signal shifts of paramagnetic molecules are a measure of the spin density at the respective nuclei. The success of the method depends heavily on the analysis of the various shift contributions which are reviewed. While traditional treatments were based on ligand-field theory, recent progress is due to quantum chemical approaches. The restrictions of the analyses are compared. Solution- and solid-state results are considered and emphasis is laid on the distinction of spin density in s- and p-type orbitals. Specific examples are nitronyl nitroxide radicals and paramagnetic metallocenes. The latter demonstrate how the analysis may depend on the spin state of the molecule.

1. Introduction

The present review is closely related to molecular magnetism which receives much attention because the assembly of neutral molecules and ions having unpaired electrons (magnetic building blocks) lead to new magnetic materials [1]. Examples are bulk magnetic materials with high Curie or Néel temperature [2], spin-crossover materials [3], photomagnets [4], chiral magnets [5], and magnetic clusters or nanomagnets [6]. The overall magnetic behavior of the building blocks is commonly traced to their spin states which are well understood [7]. However, since the desired new magnetic properties arise from the interaction between the unpaired electrons of the building blocks, a key question is: What happens on the way from one building block to the next? Actually, the unpaired spins are usually not localized on one atom, for instance, on the transition metal of a coordination compound. The metal atom must rather be regarded as a spin source from which the spin is transferred partially to the atoms of coordinated ligands. The fraction of a spin is termed spin density, which is usually given in atomic units (a.u.) to emphasize the fractional character. It may also be quoted per volume ($Å^{-3}$) to indicate that spin density is

* Corresponding authors.
E-mail addresses: kaupp@mail.uni-wuerzburg.de (M. Kaupp), f.h.koehler@lrz.tu-muenchen.de (F.H. Köhler).

0010-8545/$ – see front matter © 2009 Elsevier B.V. All rights reserved.
doi:10.1016/j.ccr.2008.12.020

associated with a shape. The spin density has a sign. That is, it orients itself parallel or antiparallel with respect to an external magnetic field or reference field. With suitable magnetic interaction, the spins may orient, thus giving the material a particular magnetic behavior.

The spin densities delocalized to the atoms at the periphery of magnetic building blocks will interact with each other upon assembly to the material. In the crystal lattice of magnetic compounds mutual spin transfer between the building blocks gives rise to parallel or antiparallel spin alignment typical for ferro- or antiferromagnetic interaction, respectively. The scenario may be comparatively well arranged as in Prussian blue-type magnets with up to six almost equivalent interactions per hexacyanometalate [8]. But it may also be complicated as in crystals of organic radicals where various close contacts between the molecules add up to the final magnetic interaction [9]. In any case, the knowledge of the spin density distribution within the building blocks, and their mutual interaction, are key points for the understanding and the design of magnetic materials. Experimental spin maps of the building blocks and of the final materials uncover the mechanism(s) generating the spin at the various atoms [10], and once this is known the synthetic chemist can modify the building blocks in order to achieve the desired magnetic interaction.

NMR spectroscopy of paramagnetic compounds [11] ("pNMR") is a method for determining the spin density distribution [10,12]. Most notably, it may be applied to solids which are magnetically undiluted, that is, to genuine magnetic materials by using established high-resolution techniques [13], while solution NMR studies are commonly used for the study of isolated magnetic building blocks. Changes of the spin density distribution upon assembling the material would then be detected by comparative studies in solution and the solid state. Other advantages of NMR spectroscopy are the relatively low cost and high resolution as compared to neutron diffraction [14] and the direct access to the sign of the spin density and again the resolution as compared to EPR spectroscopy [15]. Note, however, that NMR and EPR provide information under complementary experimental conditions because of the different electron relaxation regimes. A review on various experimental methods for the determination of spin densities is in progress [16].

As outlined below, the conversion of NMR data to spin densities is not always straightforward, due to a variety of contributions to the observed chemical shifts. The analysis may be hampered by missing data from other measurements. Also, the signal assignment of complicated ^{1}H and ^{13}C NMR spectra (and hence the assignment of the spin densities) to specific nuclei may be ambiguous, and sometimes the signals may not be detected at all because they appear in unexpected spectral ranges or because the nuclear relaxation is unfavorable. In these and other cases, it is highly desirable to theoretically reproduce or predict the NMR data and to relate them to the spin densities. This requires to go beyond the usual formalism of chemical shift tensors for diamagnetic systems (see, e.g. Ref. [17] and references therein). There have thus been substantial efforts over the past decade to compute NMR chemical shifts of open-shell (paramagnetic) species quantum chemically, usually within the framework of density functional theory (DFT). Initial studies were often restricted to the contact shifts only, which are sometimes accessible in a relatively straightforward way from computed isotropic hyperfine coupling constants [18,19], or to the anisotropy contributions from anisotropic hyperfine couplings [20]. Recently, a more general quantum-chemical framework has been developed that allows access to all relevant terms, including those beyond the contact term, and for the entire shift tensors, in a first-principles approach [21–25]. Here we will draw attention to these recent developments and describe the state-of-the-art situation of the interplay between experiment and theory of paramagnetic NMR signal shifts, and how these may be used to extract the spin density distribution in open-shell compounds.

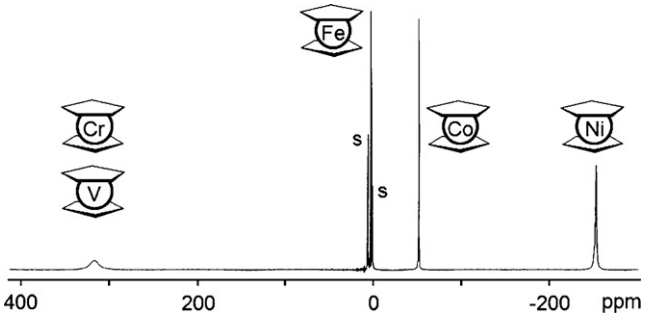

Fig. 1. ^{1}H NMR spectrum of a mixture of Cp_2V, Cp_2Cr, Cp_2Fe, Cp_2Co, and Cp_2Ni dissolved in toluene-d_8 at 32 °C. The signals of Cp_2V and Cp_2Cr coincide; S = residual proton signals of the solvent.

2. Theoretical background

2.1. General formalism

The NMR signals of paramagnetic compounds are usually much broader and more shifted than those of their diamagnetic analogues. A typical example is given in Fig. 1 which shows the ^{1}H NMR spectrum of a mixture of vanadocene (S = 3/2), chromocene (S = 1), cobaltocene (S = 1/2), nickelocene (S = 1), and diamagnetic ferrocene. The signal broadening is due to the effect of the electron spin on the nuclear spin relaxation [26] while the signal shift can be thought of as being mainly determined by the average local magnetic field of the unpaired electrons which in turn is related to the spin density.

The formalism of the chemical shifts of open-shell magnetic compounds has been developed over decades and is described in several text books [11,12]. Here we will not follow the course of the historical developments, which were often formulated within the framework of ligand-field theory, with recourse to spin susceptibilities as intermediate quantities, and with the point-dipole approximation. Instead we would like to start from a rather compact formalism that has been outlined recently within a quantum chemical framework [22–25]. This description has the advantage of containing all terms derived previously in a compact representation, based on the terms of the EPR spin Hamiltonian. The formalism allows straightforward inclusion of the effects of zero-field splitting (ZFS) for systems with S > 1/2 [25], and it is currently the most suitable basis for quantum chemical calculations. We will, however, identify wherever possible the relation to the terms appearing in the more traditional treatments [11,12,27]. For simplicity we will outline mainly the formalism for systems with S = 1/2 [22,23], where ZFS is absent. Following the derivation of Moon and Patchkovskii [22], the shift tensor of nucleus N at temperature T, $\boldsymbol{\delta}_T(N)$, for a system with S = 1/2, without thermally accessible electronically excited states, is given by Eq. (1). Hrobárik et al. [24] showed that for small ZFS contributions, this equation provides also excellent results when used in DFT calculations of ^{1}H and ^{13}C shifts for metallocene complexes with S > 1/2 (see below). When ZFS effects are large, the extended formalism of Pennanen and Vaara [25] has to be used (see further below).

$$\boldsymbol{\delta}_T(N) = \boldsymbol{\delta}_{orb}(N) + \frac{S(S+1)\beta_e}{3kT\gamma(N)}\mathbf{g}.\mathbf{A}^{\dagger}(N) = \boldsymbol{\delta}_{orb}(N) + \boldsymbol{\delta}_{HF,T}(N) \qquad (1)$$

In Eq. (1), S is the spin multiplicity, β_e the Bohr magneton, $\gamma(N)$ the nuclear gyromagnetic ratio, and $\mathbf{g}$ and $\mathbf{A}$ are the g- and hyperfine tensors, respectively. $\boldsymbol{\delta}_{orb}(N)$ is the orbital part of the shift tensor. It is formally temperature-independent and analogous to the

Table 1
Terms contributing to isotropic and anisotropic chemical shifts for systems with S = 1/2[a].

	Term	Label	Traditional assignment	
Isotropic contributions				
$\delta_{T,iso}$	$g_e A_{FC}$[b]	A	A–C: $\delta_{FC,iso}$ or $g_e f_s A_s$[f]	A–C: Contact shift, term to extract information on the isotropic spin density of the atom
	$g_e A_{PC}$	B		
	$\Delta g_{iso} A_{FC}$	C		
	$1/3 * Tr(\Delta\tilde{\mathbf{g}} \cdot \boldsymbol{A}_{dip})$[c]	D	$\delta_{SD,iso}$	Spin dipolar shift
$\delta_{orb,iso}$			$\delta_{dia,iso}$	Diamagnetic (or orbital) shift
Anisotropic contributions				
$\boldsymbol{\Delta\delta}_T$	$g_e \mathbf{A}_{dip}$[d]	E	E–H: $g_e f_p A_p$[f]	E–H: Term to extract information on the spin density in p-type orbitals of the atom
	$g_e \mathbf{A}_{dip,2}$	F		
	$\Delta g_{iso} \mathbf{A}_{dip}$	G		
	$A_{FC} \Delta\tilde{\mathbf{g}}$	H		
	$\Delta\tilde{\mathbf{g}} \cdot \boldsymbol{A}_{dip} - 1/3 * Tr(\Delta\tilde{\mathbf{g}} \cdot \boldsymbol{A}_{dip})$[e]	I	[g]	Spin dipolar shift
$\boldsymbol{\Delta\delta}_{orb}$			$\boldsymbol{\Delta\delta}_{dia}$	Diamagnetic (or orbital) shift

[a] Cf. Refs. [23,24]. A more complete list for any spin multiplicity, with contributions to anti-symmetric tensor values, and with classification in terms of fine structure constant, is provided in Ref. [25].
[b] Leading contribution to $\delta_{T,iso}$ in the case of covalent bonding.
[c] Isotropic "spin dipolar" or "pseudocontact" shift.
[d] Leading contribution to $\boldsymbol{\Delta\delta}_T$ in the case of covalent bonding.
[e] Anisotropic "spin dipolar" or shift.
[f] See Ref. [29] and Eq. (2) below.
[g] A traditional assignment does not seem to exist.

shift of diamagnetic closed-shell compounds, except that it applies specifically to the given open-shell system. In experimental studies, $\boldsymbol{\delta}_{orb}(N)$ is typically approximated by the value measured for a closely analogous diamagnetic compound, to be able to extract the temperature-dependent hyperfine shift, $\boldsymbol{\delta}_{HF,T}(N)$ (second term on the right-hand side of Eq. (1)). The validity of this assumption can nowadays be evaluated by explicit DFT calculations (see below). $\boldsymbol{\delta}_{orb}(N)$ is often termed diamagnetic shift, $\boldsymbol{\delta}_{dia}(N)$ (cf. Table 1). However, as this may lead to confusion with the distinction between diamagnetic and paramagnetic shifts in the Ramsey formalism for diamagnetic molecules (see, e.g., ref. [17] and references therein), we will in the following use the term orbital shift.

As can be seen from Eq. (1), the explicitly temperature-dependent hyperfine shifts, $\boldsymbol{\delta}_{HF,T}(N)$, that make shifts of open-shell systems often so different from their closed-shell analogues, involve the g- and A- (hyperfine) tensors also relevant for EPR spectroscopy. More correctly, both $\mathbf{g}$ and $\mathbf{A}$ are general 3×3 matrices that are made up from a scalar (an isotropic value or a zeroth-rank tensor), from a true anisotropic symmetrical second-rank tensor accounting for g- and A-tensor anisotropies, respectively, and from a first-rank asymmetric tensor we will not consider much further here (it does not affect the shifts yet may give a small contribution to spin relaxation processes). The hyperfine shift, $\boldsymbol{\delta}_{HF,T}(N)$, is obtained after taking the matrix product of $\mathbf{g}$ and the transpose of $\mathbf{A}$ (and multiplying by the temperature-dependent prefactor). This multiplication gives a variety of terms, some of which are only isotropic, some are only anisotropic, and one is both (the antisymmetric rank 1 shift tensor contributions affect spin relaxation rates but not the observed shifts and will not be discussed further). Table 1 collects and characterizes these terms [23–25]. Based on this formalism, the Table also identifies the best definitions of the contact and spin dipolar (or "pseudocontact") shifts figuring in the usual interpretation of the isotropic shifts in solution, as well as the contributions to the anisotropic shift tensors accessible in solid-state spectra (we note in passing that $\boldsymbol{\delta}_{orb}(N)$ contributes both to δ_{iso} and to the shift anisotropy $\boldsymbol{\Delta\delta}$).

For a detailed breakdown into the terms in Table 1, $\mathbf{g}$ is separated into $(g_e + \Delta g_{iso})\mathbf{1} + \Delta\tilde{\mathbf{g}}$, i.e. into the isotropic value g_e of a free electron, and the isotropic and anisotropic parts Δg_{iso} and $\Delta\tilde{\mathbf{g}}$, respectively, of the "g-shift" matrix $\Delta\mathbf{g}$ that marks the differences between the free electron and that in a compound where spin-orbit coupling may occur. Similarly, the A-matrix is made up from the terms $\mathbf{A}(N) = (A_{FC}(N) + A_{PC}(N))\mathbf{1} + \mathbf{A}_{dip}(N) + \mathbf{A}_{dip,2}(N) + \mathbf{A}_{as}(N)$. $A_{FC}(N)$ is the isotropic Fermi-contact term, $\mathbf{A}_{dip}(N)$ the dipolar hyperfine tensor. $A_{PC}(N)$ is the so-called pseudo-contact term (EPR notation) arising from spin-orbit contributions to the isotropic hyperfine coupling constant, and $\mathbf{A}_{dip,2}(N)$ is a corresponding spin-orbit contribution to the hyperfine anisotropy. The term $\mathbf{A}_{as}(N)$ is an anti-symmetric (rank 1) spin-orbit contribution. $\mathbf{1}$ is the 3×3 unit matrix.

One arrives at overall nine terms contributing to the hyperfine shifts for S = 1/2, of which four (A, B, C, D in Table 1) contribute to the isotropic shift, and five (E, F, G, H, I) to the shift anisotropy. Term D of the isotropic shift (analogously term I of the anisotropy) is usually called the "spin dipolar" (or sometimes "pseudocontact") shift. It plays an important role in attempts towards structure determination by pNMR (see below). While one might typically consider only term A as the "contact" shift, it appears more reasonable to use the sum of A and terms B and C. The latter two terms may become non-negligible in the case of a particularly large deviation of the isotropic g-value from g_e or of a particularly large pseudocontact contribution to the isotropic hyperfine coupling constant, respectively. These are two different manifestations of large spin-orbit effects. However, A is the leading and dominant part of the contact shift whenever appreciable spin density is present at the nucleus of interest. Note that at the given theoretical level (up to $\mathcal{O}(\alpha^4)$ in the fine structure constant), the pseudocontact contribution to the isotropic hyperfine coupling ($g_e A_{PC}$, term B) contributes to $\delta_{FC,iso}$ and not to $\delta_{SD,iso}$. To avoid confusion here, the name "spin dipolar shift", $\delta_{SD,iso}$, seems thus preferable over "pseudocontact shift" for term D.

Similarly, term E dominates typically the shift anisotropies, albeit terms F–I may also contribute non-negligibly under certain circumstances. This becomes important when trying to derive p-orbital spin densities from the shift anisotropies (see below).

For S > 1/2, in the extended formalism of Pennanen and Vaara [25] one takes the product between $\mathbf{g}$ and $\mathbf{A}$ in the spin eigenstates of the ZFS Hamiltonian, thus having to lower the overall symmetry

of the problem. As a consequence, the originally purely anisotropic terms E–H acquire a non-negligible isotropic character. Moreover, the term arising from the product between g_e and $\mathbf{A}_{as}(N)$ is not purely antisymmetrical (rank 1) but contributes as well to the regular shift anisotropy (rank 2) [25].

Many of the terms showing up in Table 1 have been known [11,12,27,28] decades prior to the paper by Moon and Patchkovskii. Similarly, the importance of ZFS contributions has been appreciated early on by Kurland and McGarvey [27] and others. The advantages of the formalism for S = 1/2 underlying Eq. (1) [22,23], and of the extended formalism of Ref. [25] for S > 1/2, is that these schemes consider all terms on equal footing, within an elegant description that is complete up to the order $\mathcal{O}(\alpha^4)$ in the fine structure constant. As we will discuss below (chapter 2.3), the importance of various terms can be checked by explicit quantum chemical computation, using this formalism.

2.2. Interpretation of shifts and extraction of spin densities

We see that those parts of the pNMR shift that are usually called contact or spin dipolar shifts, etc., may be composed of a number of terms, and of even more terms when ZFS becomes important for S > 1/2. In most cases, term A based on $g_e A_{FC}$ nevertheless dominates isotropic shifts, whereas term E based on $g_e\mathbf{A}_{dip}$ dominates the shift anisotropies. If these terms are relatively small for some reason, the "dipolar" shift terms D and I based on $g_e\mathbf{A}_{dip}$ may become important on a relative scale. In the case of S > 1/2, the ZFS-related terms (see above) may matter as well. For the isotropic shift, terms A–C may be small if there is no direct bonding pathway from the paramagnetic center to the nucleus in question so that a direct transfer of isotropic spin density to that nucleus, either by spin delocalization or by spin polarization, becomes less favorable. Then the spin dipolar term $\delta_{SD,iso}$ (Table 1) may be viewed as providing a "through-space" mechanism, due to the combined involvement of hyperfine and g-anisotropies.

2.2.1. Spin in s orbitals from isotropic signal shifts

If we may ascertain in some way (either by experiment or computation) that the contact shift (more precisely the sum of terms A and C) dominates δ^{iso}, we may extract information on the spin density $\rho_s(N)$ at nucleus N. It is related to the isotropic hyperfine coupling, $A_{FC}(N)$, via

$$A_{FC}(N) = \frac{4\pi}{3S} g_{iso}\beta_e\gamma(N)\rho_s(N) \quad (2)$$

(the equation pertains to the substate with highest projection of spin). The relation to the Fermi contact shift ($\delta_{FC,T}(N)$; cf. Table 1) is then

$$\rho_s(N) = \frac{9kT}{4\pi g_{iso}^2\beta_e^2(S+1)}\delta_{FC,T}(N), \quad (3)$$

keeping in mind the possible involvement of other terms in Table 1 or of ZFS contributions in the case of S > 1/2 (see above). For convenience we henceforth skip the notations (N) and T. It is common practice to convert the experimental data to 298 K.

ρ_s may feature contributions from all molecular orbitals with some s-orbital character on atom N. It seems important to note here, however, that ρ_s is the spin density at one particular point in space, that is, at the nuclear position. While one may be tempted to equate ρ_s to a spin density of the atom in question, there is a caveat to this: as is well known from isotropic EPR hyperfine coupling constants (see, e.g., Ref. [30] and literature cited therein), the spin density at the nucleus may be affected appreciably by spin polarization of the s-type core and valence orbitals around this atom. As an example from EPR, spin density at a 3d transition metal nucleus may be affected significantly by the spin polarization of the 2s and 3s core shells [31]. In the case of singly occupied molecular orbitals with little or no s-character at the metal, this will lead to negative spin density at the nucleus even if the integrated atomic spin density (in the 3d shell) is positive. Similarly, it is well known that in planar organic π-radicals, the spin polarization of the 1s and 2s shells at carbon, oxygen or nitrogen by the π-type singly occupied molecular orbital will be decisive for the spin densities at the nuclei within the π-system [30]. Valence-shell spin polarization is responsible for the spin density of substituent atoms to such π-radicals lying in the nodal plane of the π-type SOMO. This spin density has frequently the opposite sign than is present at the nucleus of the framework atom to which the substituent is bonded. Similar spin polarization mechanisms apply to the observed isotropic shifts in pNMR studies. This has to be kept in mind when discussing chemical bonding and spin delocalization based on $\delta_{FC,T}$. Nevertheless, useful correlations between spin densities at certain nuclei and integral atomic spin density distributions are known that may be exploited. One example is the well-known McConnell relationship for the hyperfine couplings at hydrogen nuclei in π-radicals [32a] which has been expanded later by including core-electron polarization and similar effects [32b,c].

In addition to the spin-orbit-related contributions discussed above (Table 1), we may sometimes have to consider the thermal population of electronically excited states. Generally, two effects must be considered here. Both the spin multiplicity and the spin delocalization/polarization between metal and ligands may be different for the thermally populated excited states compared to the ground state. The latter effect would occur regardless of whether the spin state changes or not. In both cases the product $T\delta_{FC,T}(N)$ in Eq. (3) is no longer constant, and the (Boltzmann-averaged) spin density becomes temperature dependent [25a,b,33].

2.2.2. Spin in p orbitals from anisotropic signal shifts

So far, we were concerned with solution NMR spectra. In the solid state, additional information on the spin distribution is available because in the (micro) crystals the orientation of the nuclei relative to the applied magnetic field is fixed (unless some rapid dynamic process is active). Usually, there is no need to study single crystals, because powder spectra can also be recorded by applying the solid-state NMR techniques that have been developed for diamagnetic compounds [13]. An example is the magic-angle-spinning (MAS) ^{13}C NMR spectrum of the $[(C_5Me_5)_2Ni]^+$ ion (S = 1/2) [34] given in Fig. 2. It shows the signal pattern of the ring carbon atoms (the methyl signal appears outside the window near −200 ppm) which can be simulated. The isotropic shift is obtained from $\delta_{iso} = 1/3\sum\delta_{ii}$ ($\delta_{ii} = \delta_{xx}$, δ_{yy}, δ_{zz} are the principal shift tensor components). In fact, it has been demonstrated that in the absence of strong intermolecular interactions in the crystal (and in the absence of intermolecular magnetic exchange [35]), the isotropic shift of a

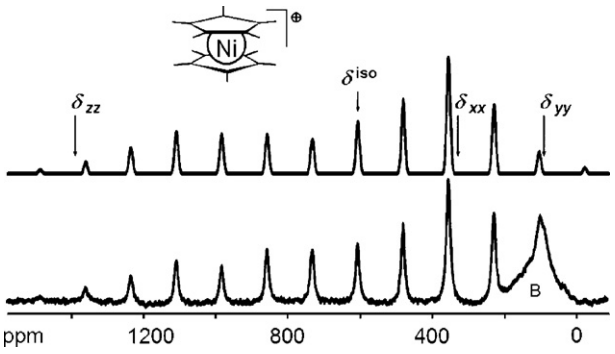

Fig. 2. ^{13}C MAS NMR spectrum of $[(C_5Me_5)_2Ni]^+[PF_6]^-$ at 28 °C. MAS frequency: 9.5 kHz; only the pattern of the ring carbon atoms is shown; bottom: experimental, top: simulated; B: background signal of the probe head; the δ_{ii} positions are fit values.

species is largely independent of whether it is tumbling freely in solution or whether it is locked in the crystal lattice [36] (contrary to a previous assertion [37]). Therefore, the isotropic contact shift contribution may be converted to ρ_s as in solution, by applying Eq. (3).

In addition, there is an anisotropic spin distribution which is reflected in the solid-state NMR spectra by the signal shift tensor and which can be characterized by the shift anisotropy, $\Delta\delta$, through

$$\Delta\delta = \delta_{zz} - \frac{1}{2}(\delta_{xx} + \delta_{yy}) \quad (4)$$

and by the asymmetry (that is, the deviation from axial symmetry), η, through

$$\eta = \frac{\delta_{yy} - \delta_{xx}}{\delta_{zz} - \delta_{iso}} \quad (5)$$

where $|\delta_{zz} - \delta_{iso}| \geq |\delta_{xx} - \delta_{iso}| \geq |\delta_{yy} - \delta_{iso}|$ [38]. Note that for a reliable analysis of the experimental spectra the heteronuclear spin coupling must be small compared to $\Delta\delta$.

In the case that $\Delta\delta_T$ is dominated by term E ($g_e\mathbf{A}_{dip}$, Table 1), the anisotropic part of the shift tensor may be related to the dipolar hyperfine coupling, $\mathbf{A}_{dip}$, at the ligand nucleus N in question. This is often taken as a signature of the spin density in the sum of the p orbitals around the ligand nucleus in question. However, experience from EPR spectroscopy suggests that matters may be more complicated: even if relatively little p-orbital spin density is located on the given ligand atom, the $\mathbf{A}_{dip}$ of this nucleus may be affected by anisotropic spin density on neighboring atoms. The situation holds particularly for those nuclei in the direct neighborhood of the paramagnetic metal center, which will experience the field created by the spin density of the metal d-orbitals. This is an exciting area, where quantum chemical calculations may in the future offer vastly improved interpretational tools. For the systems discussed in the present review the point-dipolar approximation is probably a reasonable one, however.

2.2.3. Impact of the spin dipolar signal shift

It follows that the precision of the spin densities ρ_s and ρ_p depends on the approximations accepted when the experimental signal shift data are processed. Another restriction of the usual procedure is evident: the desired contact shift, δ^{con}, is obtained after subtracting the orbital and spin–dipolar components, δ^{orb} and δ^{SD}, from the experimental signal shift. One usually approximates δ_{orb} (for both isotropic and anisotropic shifts) by values obtained for diamagnetic compounds that are isostructural to the paramagnetic systems studied. Given that δ_{orb} is usually smaller than the leading terms (often δ_{FC} for δ_{iso}), this may often be a reasonable approximation (see below).

For the spin–dipolar interaction, it has been common practice [11,12] to calculate the contribution to the isotropic shift within the point-dipole approximation, using Eq. (6).

$$\delta_{SD,iso,M} = \frac{\beta_e^2 S(S+1)}{9kT} \frac{3cos^2\Theta - 1}{r^3} f_S(g, D) \quad (6)$$

The second of the three factors in Eq. (6) is the well-known geometrical component of dipolar interactions. Here the vector $\boldsymbol{r}$ joins the center of the spin source (typically the metal atom) and the relevant nucleus, while θ is the angle between $\boldsymbol{r}$ and the magnetic axis of the molecule. The last factor is a function of the g tensor and the ZFS which depends on the spin state. The simplest case is S = 1/2 for which $f_S = (g_{||}^2 - g_{\perp}^2)$ [37] when the molecule has axial symmetry. The shift sign convention of the earlier work such as Refs. [27,37] has meanwhile been reversed. The theory had been extended to S > 1/2 (with isotropic D) arriving at the expressions summarized in Eq. (6) [27] and to orbital contributions [28c,d]. To go beyond the point-dipole approximation, corrections for ligand-centered dipolar shifts, $\delta_{SD,ido,L}$, have been addressed theoretically [27,39]. As indicated above, explicit calculation of full $\delta_{SD,ido}$ by accurate quantum chemical methods without drastic approximations has become possible, for any S. In this case, distinction between metal and ligand contributions is not necessary but can of course be made a posteriori. The actual role of the spin dipolar shifts for many specific examples is an interesting question for future research (see below).

Coming back to the shift anisotropy of solid-state NMR signals, it is now obvious that it also contains some dipolar contribution (term I) which must be separated before term E (or better the sum of terms E–H; Table 1) may be used to evaluate anisotropic spin density distribution around the nucleus in question. Experimentally, this can be done by fitting the spectra directly with the calculated data of the total electron–nuclear interaction tensor and the g tensor [40]. Alternatively, the terms for the anisotropic parts of the metal- and ligand-centered dipolar shifts, as well as the orbital shift anisotropy, can be subtracted from the total shift anisotropy [41]. This will again be an area where explicit quantum chemical calculations should become extremely helpful.

2.3. Explicit density functional calculations

As indicated above, the formalism of Eq. (1) [22,23], and also the extended treatment for S > 1/2 [25], are particularly suited for calculations by quantum chemical methods. Given that such calculations will often deal with relatively large molecular systems, frequently containing one or more transition metal atoms, the best cost/accuracy ratio is currently provided by density functional theory (DFT), and we will in the following focus exclusively on DFT methods.

All terms summarized in Table 1, resulting from a treatment correct to order $\mathcal{O}(\alpha^4)$ in the fine structure constant, have been implemented into computer programs within a DFT framework [21–23], including the recent extensions to S > 1/2, with ZFS contributions [24,25]. The only small caveat so far is, that at $\mathcal{O}(\alpha^4)$, spin-orbit corrections to $\boldsymbol{\delta}_{orb}$ should be included. While these have been implemented for diamagnetic systems [42], an implementation for open-shell species is still lacking. However, experience established in the last decade for such "spin-orbit" shifts of diamagnetic systems gives clear guidelines on when such terms could matter [43]. The current DFT implementations of pNMR shifts use perturbation theory based on the Breit-Pauli Hamiltonian to account for any spin-orbit contributions. For systems containing very heavy atoms, this may not be accurate anymore, and thus more complete (and computationally demanding) relativistic treatments may have to be used. Work on such approaches is being pursued in a number of laboratories.

Considering Eq. (1), we see that calculation of $\boldsymbol{\delta}_{HF,T}$ requires computation of g- and A-tensors. DFT calculations of these EPR parameters have been subject to substantial development over the past decade, including work on both organic radicals and transition metal complexes [17]. The same holds for the ZFS in the case of S > 1/2 (see Ref. [44] for an interesting recent DFT implementation). That is, the treatment of pNMR parameters benefits greatly from developments made on the EPR side. This holds also for the transfer of know-how on basis sets, exchange-correlation functionals, and other computational details. In particular, isotropic hyperfine coupling constants may depend significantly on the functional and basis set, and thus care has to be taken to obtain quantitatively reliable results. Computations of $\boldsymbol{\Delta g}$ and of spin-orbit corrections to $\mathbf{A}$ in turn require accurate treatments of the spin-orbit matrix elements involved in the second-order perturbation treatment (or in a variational relativistic treatment). This is also an area where significant progress has been made recently [45,46].

The $\boldsymbol{\delta}_{orb}$ term may be computed in analogy to the diamagnetic case, with the main difference that the second-order perturbation method has to be formulated for a spin-polarized open-shell treatment [21–25] (this is closely analogous to a perturbation treatment for the g-tensor [45] and thus easily generalized). $\boldsymbol{\delta}_{orb}$ may thus be computed explicitly for paramagnetic compounds, and one may check the frequently made assumption that this term may be taken (see above) from a structurally related diamagnetic compound. Notably, for the computation of $\boldsymbol{\delta}_{orb}$, one has to deal with the gauge-origin problem that is well known for the diamagnetic case. A number of distributed-gauge methods are available. The best-known are the "gauge-including atomic orbital" (GIAO) [47] and "individual gauges for localized orbitals" (IGLO) [48] approaches. While the gauge-origin problem pertains also to the g-tensor (not to the A-tensor), it is less severe, and often a common gauge, e.g. at the transition metal center, will suffice in such cases.

While the terms A and E in Table 1 may in principle be obtained by using any quantum chemical program that allows the computation of (nonrelativistic) hyperfine tensors, some of the other terms have so far been implemented only into a few programs. We note in particular the reports in Refs. [21–25] for further information. In fact, the nature of Eq. (1) (and of the extended formalism in Ref. [25]) allows the individual terms to be obtained at different computational levels. For example, one may choose to use GIAOs for $\boldsymbol{\delta}_{orb}$ but not for the g tensor. Or one may use a so-called hybrid DFT functional for the A-tensor but not for the g-tensor or $\boldsymbol{\delta}_{orb}$ (the exact-exchange admixture of a hybrid functional is more important for A_{iso} than for the other terms in Eq. (1) or Table 1 [49]). In fact, the different terms have even been obtained from different computer programs and were then combined to provide $\boldsymbol{\delta}_T$.

3. Combination of experimental NMR studies and quantum chemical calculations to obtain spin density distributions

3.1. Nitronyl nitroxides

There is an organic side of molecular magnetic materials which is dominated by the nitronyl nitroxides. These radicals have been shown to become low-temperature bulk magnets as such [50] or after coordination to paramagnetic transition metal ions [51]. This has led to a rich chemistry through variation of their substituent R (Fig. 3), and hence there was a need to understand how the spin-density distribution changes with R. Solid-state NMR spectroscopy has been shown to be very efficient for this purpose, and its performance as compared to other methods has been described [52].

As starting point for the comparison of experimental and theoretical NMR data, these organic radicals are most appropriate because their ground state is S = 1/2, and excited states are thermally not accessible. Due to the small spin-orbit coupling of nitrogen, oxygen and carbon, the g factor anisotropy is very small. There is no zero-field splitting. Therefore the analysis of the NMR data is greatly simplified. One may thus safely assume that the contact shift dominates $\boldsymbol{\delta}_{HF,T}$ in form of term A (Table 1). On the experimental side, $\delta_{FC,iso}$ may then be obtained by subtracting $\delta_{orb,iso}$ from δ_{iso}^{exp} at the given temperature T and be used to obtain ρ_s from Eq. (3). It is sufficient to set $g_{iso} = g_e = 2.0023219\ldots$ because the isotropic g value of the nitronyl nitroxides is close to 2.007 [52,53] so that the error is only 0.5%. From the bulk radicals studied so far by ^{1}H, ^{2}H, ^{13}C, and ^{31}P MAS NMR spectroscopy [54], those are selected here (see Fig. 3) whose contact shifts have also been calculated by DFT methods [21,55]. The comparison of the results is summarized in Table 2. The experimental ρ_s^{MAS} values were obtained through Eq. (3) from the isotropic contact shifts which in turn were referenced relative to the shifts of the diamagnetic analogues. A better referencing method would be to study the temperature dependence of the signal shifts and to determine the temperature-independent shift (corresponding to $\delta_{orb,iso}$) from the straight line in a shift-versus-T^{-1} diagram. However, nitronyl nitroxides are thermolabile so that the routinely accessible temperature range is too small for an acceptable error limit. The experimental contact shifts have thus contributions that would contaminate the ρ_s^{MAS} values. These contributions are usually small, but may occasionally reach a few percent. The spin densities ρ_s^{DFT1} in Table 2 are those reported in Ref. [52], while the ρ_s^{DFT2} values were obtained after converting the theoretical contact shifts of Refs. [21,55] with Eq. (3).

There are some useful conclusions to be drawn from Table 2. (i) When spin densities are not available because the NMR signals are difficult to observe, quantum chemistry suggests precise spectral ranges as, for instance, in the case of C2 of the nitronyl nitroxides. Yet so far, all NMR attempts to detect C2 failed due to excessive signal broadening even after 99% enrichment of ^{13}C [56]. (ii) The calculations may be the only means of assigning spin densities or shifts to specific atoms. Examples are the values for the axial and equatorial methyl groups. (iii) The theoretical and experimental results are in good to acceptable agreement. (iv) The spin densities ρ_s^{DFT2} calculated from the theoretical contact shifts are in better accord with the experimental ρ_s^{MAS} values than the spin densities ρ_s^{DFT1}, especially for the hydroxy derivatives **3** and **4**. Apart from differing basis sets, this is mostly due to the fact that for the ρ_s^{DFT2} values of **2**–**4**, water molecules were added in order to mimic hydrogen bonding (Table 2, footnote [a]). Intramolecular hydrogen bonding was also considered for the ρ_s^{DFT1} values of **2**, which are good. In contrast, the intermolecular hydrogen bonding in **3** and **4** has not been considered for the respective ρ_s^{DFT1} values, and hence they are less accurate. It follows that the inclusion of environmental effects in the calculation generally improves the results, similar to the case of EPR hyperfine couplings of organic radicals. So far, no nitronyl nitroxide has been studied by both NMR and PND, but the experimental spin densities are in the same range. An example is the PND study of the first organic ferromagnet [57].

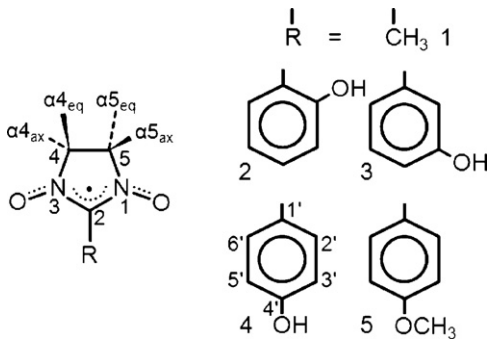

Fig. 3. Selected nitronyl nitroxide radicals **1**–**5**.

3.2. Metallocenes

Metallocenes figure at the very beginning of molecule-based magnetic materials when it was found [58] that they react with electron-poor organic π compounds such as tetracyanoethylene to form stacked compounds. These stacks may experience magnetic interaction with spin alignment at low temperature. Since then, a great variety of organic π compounds and bis(chalcogenate)metalates have been incorporated in the stacks as counterions of the metallocenium ions [59]. The mechanism of the magnetic interaction has been discussed controversially: first, it was proposed [58] that excited states of the metallocenium ion mix into the ground state thereby inducing a high-spin ground state. Later, exchange of positive and negative spin in the π systems of the organic radical and the ligands of the metallocenium ion, respectively, was suggested to be responsible for the ferromagnetic

Table 2
Comparison of the experimental and theoretical spin densities[a] at the hydrogen and carbon atoms of the nitronyl nitroxides **1**–**5**.

	1	**2**			**3**			**4**			**5**[b]		
	ρ_s^{MAS}	ρ_s^{DFT2}	ρ_s^{MAS}	ρ_s^{DFT1}	ρ_s^{DFT2}	ρ_s^{MAS}	ρ_s^{DFT1}	ρ_s^{DFT2}	ρ_s^{MAS}	ρ_s^{DFT1}	ρ_s^{DFT2}	ρ_s^{MAS}	ρ_s^{DFT2}
$C\alpha4_{ax}$	9.82	7.22	10.3	10.59	10.62	9.3	12.00	8.52	9.4	5.83	9.24	9.24	9.61
$C\alpha5_{ax}$	10.12	7.37	6.1	6.95	7.193	8.9	9.58	8.40	10.9	7.14	9.76	10.01	9.31
$C\alpha4_{eq}$	4.87	3.97	3.38	3.39	3.71	4.85	3.15	3.33	2.56	2.11	2.58	2.77	2.87
$C\alpha5_{eq}$	5.55	4.13	3.01	2.51	2.84	4.85	3.67	3.15	3.04	2.87	2.86	3.54	2.64
C2	[c]	−17.24	[c]	−33.93	−28.71	[c]	−42.82	−32.00	[c]	−42.68	−31.37	[c]	−30.69
C4	−6.18	−3.67	−7.23	−7.65	−6.84	−6.85	−8.01	−5.90	−3.84	−5.90	−5.77	−4.77	−5.72
C5	−6.48	−3.60	−3.32	−3.86	−3.69	−6.05	−7.54	−5.93	−6.20	−7.06	−5.72	−5.84	−5.74
C1′	3.83	1.94	[c]	8.16	6.70	4.98	12.11	6.37	5.10	12.43	6.22	5.31	6.04
C2′			−3.42	−5.55	−4.00	−2.06	−7.02	−2.58	−1.92	−7.69	[d]	−2.24	[d]
C3′			1.07	1.89	0.95	1.45	5.30	1.44	1.11	4.35	1.49	1.27	1.44
C4′			−0.75	−2.83	[d]	−1.17	−6.42	[d]	−1.22	−5.48	−1.68	−1.50	−1.65
C5′			0.69	2.18	[d]	1.32	5.04	[d]	1.11	4.44	[d]	1.37	[d]
C6′			−2.88	−4.94	[d]	−2.67	−7.78	[d]	−2.23	−8.00	[d]	−2.41	[d]
Hβ4/5	−0.13	−0.10[f]	−0.12[e]	−0.06	−0.11	−0.13[e]	−0.09	−0.14	−0.14[e]	−0.10	−0.12	−0.14[e]	−0.12
H1′	−1.94	−1.45											
Hα2′/6′			0.19	0.36	[d]	0.32	0.73	[d]	0.23[e]	0.64	[d]	0.30	[d]
Hα3′			−0.09[e]	−0.18	−0.10				−0.10	−0.40	−0.09	−0.11	−0.10
Hα4′			0.19	0.31	0.24	0.29	0.70	0.33					
Hα5′			−0.10[e]	−0.20	[d]	−0.11	−0.40	−0.10	−0.10	−0.37	−0.09	−0.11	−0.10
OH/OD			−0.20	−0.62	−0.50	0.02	−0.04	−0.01	−0.09	0.15	−0.11		

[a] All data in a.u. × 10^{-3}, ρ_s^{MAS} and ρ_s^{DFT1} data from Ref. [52], ρ_s^{DFT2} calculated from the theoretical contact shifts of Refs. [21,55] for **1**, **2**(H_2O), **3**·$(H_2O)_2$, **4**·$(H_2O)_2$, and **5**(H_2O).
[b] No theoretical data of the methoxy group available.
[c] Not observed.
[d] Not reported.
[e] From solution NMR data.
[f] From mean shift value of axial and equatorial methyl protons.

interaction [60]. Accordingly, the study of spin densities was an issue. The latter mechanism has been confirmed initially with solution-state NMR spectroscopy [61]. At that time elaborate substitution of the metallocenes had to be realized for establishing positive or negative spin density in the ligand π systems. It is, however, more convenient to study simple metallocenes by solid-state NMR spectroscopy [34,41,62], because then spin in the s and p orbitals of the ligand atoms can be studied selectively and simultaneously.

To keep the analysis simple, the parent metallocenes $(C_5H_5)_2M$ or Cp_2M (M=V, Cr, Mn, Co, Ni), see Fig. 1, have been selected for an initial detailed comparison between experimental and computed paramagnetic ^1H and ^{13}C NMR signal shifts [23–25], although decamethylmetallocenes were needed (to meet the required reducing power) for the synthesis of the magnetic materials mentioned above.

A summary of the results is given in Table 3. Experimental isotropic ^{13}C and ^1H shifts from liquid- and solid-state measurements are compared with DFT-computed values from Refs. [24,25], respectively. The two sets of calculations differ in two main aspects: a) They have used different exchange-correlation functionals. To enable best comparison, we have selected for the Table the most similar hybrid-functional results available, that is PBE0 results with 25% exact exchange in the case of Ref. [25] and the BPW91-30HF results with 30% exact exchange from ref. [24]. b) The calculations of Pennanen and Vaara [25] used the extended formalism including the *a priori* treatment of ZFS effects. On the other hand, the calculations of Hrobarik et al. [24] used the original formalism for S = 1/2 of refs. [22,23] and applied ZFS corrections *a posteriori*. As these turn out to be very much smaller than those of Ref. [25], they are not given in the Table. Those calculations extend also to the S = 1/2 case Cp_2Co (earlier results by Pennanen and Vaara [23] used no hybrid functionals and have not been included in the comparison).

Ignoring for a moment the ZFS-related terms (the sum of terms 2,4,7,8 in Ref. [25]) one sees that the two sets of DFT calculations agree well in their overall results and for most individual contributions, in spite of the somewhat different functionals used. Notable differences pertain to the contact contributions to the ^{13}C shifts in Cp_2Ni, which are larger by ca. 160 ppm in the PBE0 results than in the BPW91-30HF data. Interestingly, this difference in term A is overcompensated by the ZFS-related terms in Ref. [25]), which sum to −200.8 ppm. As a result, the two calculations provided rather similar total shifts. The very small ^{13}C contact term for $^6Cp_2Mn$ is more negative by about 20 ppm at the BPW91-30HF level, and the total shifts differ by a similar amount. The orbital shifts in Ref. [24] have been obtained at BP86 GGA level and are about 1 ppm larger for the ^1H case than the PBE0 values of Ref. [25]. While this would be a notable difference for a diamagnetic system, it remains negligible due to much larger differences in the other terms. Agreement with experiment is reasonable in most cases yet far from perfect. The most important deficiencies of both sets of DFT calculations are in their approximate exchange-correlation functionals. This becomes obvious when comparing results in these two papers that were obtained with different functionals. These show, not surprisingly, an appreciable dependence of the contact shifts on the functional.

The very large negative −201 ppm contribution to the ^{13}C shift from ZFS-related terms in Cp_2Ni is the most striking result arising from the extended formalism of Pennanen and Vaara [25] (term 2 of Ref. [25] dominates). The magnitude of this term would be sufficiently large that it needs to be taken into account even in semi-quantitative estimates of spin densities from the isotropic shifts (although differences between different functionals for the contact terms may still be in the same order of magnitude). We note, however, that the ZFS-related contributions in Ref. [25] depend on the accuracy with which the ZFS tensor has been computed. It turns out (Table 2 in supporting information to Ref. [25]) that a significantly too large ZFS was obtained for Cp_2Ni (104.4 cm^{-1} at PBE0 level compared to ca. 30 cm^{-1} experimentally), whereas the *D*-value for Cp_2Cr was too small in absolute value (−2.0 cm^{-1} at PBE0 level compared to −15.1 cm^{-1} experimentally). Taking the experimental ZFS-tensor to carry out the diagonalization of **g**·**A**, one arrives [64] at ZFS-related contributions (sum of terms 2,4,7,8 in Ref. [25]) to ^{13}C shifts of −55.4 ppm for Cp_2Ni and of 1.9 cm^{-1} for Cp_2Cr. The corresponding contributions to ^1H shifts are 0.3 and

Table 3
Comparison of experimental and theoretical ^{13}C and ^{1}H shift data (in ppm vs. TMS at 298 K) and spin densities (in a.u. × 10^{-3}), of the 3d metallocenes, and breakdown of the DFT results of Refs. [24,25] (*in parentheses*) into different contributions[a].

	δ^{liq}	$\delta^{MAS,iso}$	ρ_s^{liq}	$\delta_{orb,iso}$	$\delta_{FC,iso}$ (A–C)[b]	$\delta_{FC,iso}$ A only[c]	ρ_s^{DFT} (A only)	$\delta_{SD,iso}$[d] (D)	$\delta_{ZFS,iso}$[e]	δ^{DFT} total[f]
^{13}C										
$^{3}Cp_2Ni$	1514[g]	1710[m]	8.64	93.3 *(94.3)*	1530.1 *(1377.2)*	1537.1 *(1381.3)*	9.73 *(8.74)*	−21.3 *(−30.6)*	−200.8	1401.2 *(1440.9)*
$^{2}Cp_2Co$	614[h]	688[m]	5.94	*(88.5)*	*(591.0)*	*(602.9)*	*(5.09)*	*(−10.4)*		*(669.0)*
$^{6}Cp_2Mn$	1274[i]	1187[n]	4.36	115.3 *(114.1)*	1707.9 *(1722.2)*	1706.1 *(1718.5)*	6.17 *(6.22)*	0.0 *(0.0)*	−2.8	1820.4 *(1836.3)*
$^{3}Cp_2Cr$	−250[j]	−225[o]	−1.88	110.2 *(106.8)*	−323.6 *(−330.4)*	−342.9 *(−348.8)*	−2.17 *(−2.21)*	−2.2 *(−2.6)*	−0.3	−215.9 *(−226.2)*
$^{4}Cp_2V$	−510[k]	−422[m]	−2.93	101.1 *(100.9)*	−523.6 *(−535.0)*	−537.2 *(−549.6)*	−2.72 *(−2.78)*	0.7 *(0.8)*	−7.4	−429.2 *(−433.3)*
^{1}H										
$^{3}Cp_2Ni$	−253[l]	−253[m]	−1.48	5.1 *(6.3)*	−246.8 *(−246.3)*	−239.7 *(−237.3)*	−1.52 *(−1.50)*	0.0 *(−0.1)*	−0.9	−242.6 *(−240.1)*
$^{2}Cp_2Co$	−51[h]	−52[m]	−0.62	*(5.2)*	*(−39.1)*	*(−38.9)*	*(−0.33)*	*(−0.4)*		*(−34.2)*
$^{6}Cp_2Mn$	−27[l]	−11[n]	0.08	6.3 *(7.4)*	−0.8 *(−22.8)*	−0.8 *(−22.9)*	0.00 *(−0.08)*	0.0 *(0.0)*	−0.3	5.2 *(−15.4)*
$^{3}Cp_2Cr$	320[l]	320[m]	1.87	5.4 *(6.4)*	305.2 *(305.2)*	302.1 *(302.4)*	1.91 *(1.91)*	0.6 *(0.6)*	0.1	311.3 *(312.3)*
$^{4}Cp_2V$	318[l]	307[m]	1.62	5.2 *(6.4)*	333.0 *(333.2)*	333.4 *(333.9)*	1.69 *(1.69)*	0.2 *(0.2)*	−2.1	336.3 *(339.9)*

[a] See Table 1 for designation of terms. All data in ppm at 298 K relative to TMS except for the ^{13}C solution data of Cp_2Mn 1274 (389 K). DFT results from Ref. [25] with PBE0 functional (summarized in the supporting information of that paper) and results from Ref. [24] (italics in parentheses) with BPW91-30HF functional (BP86 for $\delta_{orb,iso}$). The *a posteriori* ZFS corrections of Ref. [24] are significantly smaller than the *a priori* values of Ref. [25] and thus omitted here. The spin densities were calculated from the signal shifts by using Eq. (3); in the case of the experimental shifts δ^{liq} and S > 1/2, Eq. (3) was expanded based on Eqs. (40), (42), (44) of Ref. [25].

[b] Sum of terms 1,3,6 in Ref. [25].

[c] Term 1 in Ref. [25].

[d] Term 9 in Ref. [25].

[e] Sum of terms 2,4,7,8 in Ref. [25]. These are the terms genuinely related to the ZFS in the extended treatment of Pennanen and Vaara.

[f] Sums of all terms, PBE0 results from Ref. [25], BPW91-30HF results from Ref. [24]. The isotropic values δ^{liq} have been obtained in the liquid state from Refs.

[g] [63a].

[h] [33].

[i] [63b].

[j] [63c].

[k] [63d].

[l] [63e].

[m] The δ^{MAS} values are those of the MAS NMR spectra from Ref. [41].

[n] [41] mean shift value of terminal and bridging ligands of the polymeric (non-sandwich) compound.

[o] The δ^{MAS} value from Ref. [24].

0.6 ppm, respectively, i.e. almost negligible. The main change compared to the data given in Table 3 would be an overall larger total ^{13}C shift of 1582.7 ppm for Cp_2Ni. Nevertheless, it is clear that ZFS contributions are significant for the ^{13}C shift of this triplet complex. Significant ZFS contributions have also been computed for the ^{13}C anisotropy in Cp_2Ni [25] (again, somewhat reduced values would arise with a realistic ZFS-tensor).

The spin–dipolar contributions to the isotropic shifts are essentially negligible for the ^1H shifts and reach 10–30 ppm for the ^{13}C shifts in Cp_2Ni and Cp_2Co (Table 3). Even for the very small isotropic ^1H shifts of $^6Cp_2Mn$, the spin–dipolar contributions remain thus of relatively little importance. Spin-orbit contributions to the contact shifts (terms B and C in Table 1) may be up to about 20 ppm (for Cp_2Cr; Table 3) for ^{13}C shifts, up to a few ppm for ^1H shifts. With the notable exception of the abovementioned ZFS terms for Cp_2Ni, term A dominates thus generally the isotropic shifts in these metallocenes, and extraction of ρ_s values from Eq. (3) appears relatively straightforward. We note in passing that estimates of the spin–dipolar and ZFS-based terms via the traditional formalism [24] and the DFT-based data in Table 3 provide partly different results. Nevertheless, the agreement between spin densities ρ_s obtained from the liquid-state NMR spectra and those obtained from the contact shifts of the DFT calculations is very good in most cases (Table 3), with the largest deviations seen for the ^{13}C shift of $^6Cp_2Mn$, where the computed spin densities reflect the larger computed than experimental shifts. No PND study is available for comparison with the data of Table 3 while the decamethylferrocenium ion has been reported recently [65]. The computational studies of Refs. [24,25] provide further analyses, e.g. of the shift anisotropies, on spin polarization and delocalization mechanisms, and on the influence of the exchange-correlation functional on the hyperfine shifts. The ^{13}C shift tensors of different spin states of the less symmetrical complex $[Cr(en)_2NH_3Br]^{2+}$ have also been analyzed in detail [25].

3.3. Other examples for the interplay between NMR spectroscopy and quantum chemical computations

The cases described in Sections 3.1 and 3.2 are not the only studies, in which quantum chemical calculations have been used to aid in the interpretation and analysis of NMR spectra of paramagnetic compounds. As our focus here is mostly on molecular magnetic materials, a full description of work that dealt with, e.g., bioinorganic chemistry or catalysis, is beyond the scope of this article. Nevertheless, we would like to mention a few studies to give a rough impression of the state of the art in the field.

In essentially all studies except of those mentioned above [21–25], the quantum chemical calculations were restricted to the computation of the contact shift contributions from the spin density at the nucleus (cf. Eq. (3)), often using DFT calculations with standard quantum chemical programs. Probably the first study of this kind were calculations of contact shifts in models for high-spin Fe^{III} in the protein rubredoxin [18a], later extended to relaxation rates dependent on the dipolar shift contribution [18b]. These types of calculations have been demonstrated to often provide excellent agreement with experiment, of course focusing on positions where one would assume the contact shifts to dominate, with appreciable applications to metalloenzyme model complexes (see, e.g., work by Oldfield and coworkers [19,20]). A recent relevant application of this type of calculation to materials in the solid state by Sheibat et al. [66] dealt with the characterization of polymorphs and of solid-state reactions of copper complexes $[CuQ_2]$ (Q = 8-quinolinol). Orbital shifts were estimated by calculations on diamagnetic $[ZnQ_2]$ complexes (at the $[CuQ_2]$ structures), and basis sets in the B3LYP-based calculations of contact shifts were only moderately large. Nevertheless, the calculations helped a) in the assignment of the spectra and b) in reproducing at least qualitatively the differences between the spectra of the α- and β-polymorphs. Very extreme shift positions obtained computationally for some carbon nuclei were in some cases not observed experimentally, very likely due to too fast relaxation of nuclei that are very close to the paramagnetic Cu centers [66]. As indicated above, this is one role that computations may play: to predict ranges in which to look for experimental signals. We mention in passing also a study of NMR shifts in ionic oxides in the solid state [67]. However, in this case the plane-wave pseudopotential methodology did not allow the explicit calculation of spin densities (and thus of contact shifts) at the nuclei. Qualitative insights were obtained from approximate consideration of spin densities at certain sites.

Last but not least, a few applications to transition metal catalysts are notable: Kervern et al. [68] used DFT calculations of contact shifts to help characterize a high-spin Fe^{II} catalyst precursor by solid-state MAS ^{13}C and ^1H spectroscopy in a powdered molecular solid (calculations were done at B3LYP level with 6-311G* basis for carbon and 6-31G* basis for hydrogen: this provided apparently sufficient accuracy for signal assignment and interpretation). Similarly, Fernández et al. [69] used B3LYP/6-311G*-based calculations of ^1H contact shifts to assign the spectra of paramagnetic Cr^{III} olefin polymerization catalysts. Correlation with experimental shifts was excellent ($r^2 = 0.97$), and it was suggested that such calculations may also allow prediction of spectra for intermediates along the catalytic pathway [69]. Mechanistic insights into the stereoselectivity of kinetic hydrolytic resolution (KHR) of epoxides by Jacobsen-type Co^{III} salen complexes were obtained similarly by a combination of NMR spectroscopy for both dia- and paramagnetic catalyst species and explicit DFT calculations of ^{13}C and ^1H shifts [70]. These calculations were done at comparable levels as those discussed in Section 3.2 for the metallocenes. That is, the orbital shifts and the spin dipolar shifts were also computed explicitly, at B3LYP level with IGLO-II basis sets for carbon and hydrogen. However, the spin dipolar shifts turned out to be small for essentially all nuclei of interest, even in the cyclohexane and *t*-butyl moieties, and thus the contact shifts dominated the agreement with experiment. Excellent correlation with the experimental data could be obtained only when optimizing the structure of the paramagnetic complexes. This led to an appreciably buckled structure of the salen ligand framework and thereby provided an explanation for the stereoselectivity of KHR. The flatter structure found by X-ray diffraction for the solid gave poor correlation with experimental shifts [70].

4. Conclusions

When aiming at establishing the spin density distribution of molecules, the NMR method has advantages such as high resolution, access to genuine magnetic materials, and low cost. These advantages can be fully realized through an appropriate analysis of the experimental signal shifts. Previous procedures passed via the magnetic susceptibilities at the molecular level in order to arrive at the electron–nuclear coupling constant which can be converted to the spin density. The basic ligand-field treatment was extended repeatedly up to a demanding level. Yet, sometimes severe assumptions had to be made whose impact still has to be clarified.

Recent developments in the quantum chemical treatment of NMR shifts of paramagnetic systems offer direct computational access to the individual terms contributing to the NMR signal shift tensors. After correlating the terms of the ligand-field and quantum chemical approaches it may be checked in detail how previous assumptions act on the various shift contributions and thus the spin densities. While organic radicals such as the nitronyl nitroxides are little affected, the numerical results of open-shell transition-metal compounds such as the metallocenes may show appreciable differences. The quantum chemical approach supports the experiment

in many ways, e.g., by assuring and even predicting the assignment of pNMR signals. Most importantly, generating spin maps of magnetic materials can be done by close interaction between theory and experiments. It is clear that we will see more direct interactions between NMR spectroscopy and quantum chemical calculations in the determination of spin-density distributions for molecular magnetic materials in the years to come. So far only the surface of the possibilities of this combination of tools has been touched upon.

Acknowledgments

A.V. Arbuznikov and R. Reviakine have contributed to the described theoretical and computational developments by the Würzburg group. The quoted work has been done in collaboration with P. Hrobarik, O.L. Malkina, and V.G. Malkin (Slovak Academy of Sciences). We are very grateful to J. Vaara and T. Pennanen for helpful discussions and for communicating unpublished data. The work of the authors described herein has been carried out within priority program SPP1137 "Molecular Magnetism" of the Deutsche Forschungsgemeinschaft.

References

[1] (a) H. Kronmuller, S. Parkin (Eds.), Handbook of Magnetism and Advanced Magnetic Materials, vol. 4, J. Wiley & Sons, Chichester, 2007;
(b) J.S. Miller, M. Drillon (Eds.), Magnetism: Molecules to Materials, vol. 1–5, Wiley-VCH, Weinheim, 2001–2005;
(c) K. Itoh, M. Kinoshita (Eds.), Molecular Magnetism, Kodasha, Tokyo, and Gordon and Breach Science Publishers, Australia, 2000;
(d) P.M. Lahti (Ed.), Magnetic Properties of Organic Materials, Marcel Dekker, New York, 1999.
[2] (a) M. Verdaguer, A. Bleuzen, C. Train, R. Garde, F. Fabrizi de Biani, C. Desplanches, Philos. Trans. R. Lond. A 357 (1999) 2959;
(b) M. Verdaguer, A. Bleuzen, V. Marvaud, J. Vaissermann, M. Seuleiman, C. Desplanches, A. Scuiller, C. Train, R. Garde, G. Gelly, C. Lomenech, I. Rosenman, P. Veillet, C. Cartier, F. Villain, Coord. Chem. Rev. 190–192 (1999) 1023.
[3] (a) J.A. Real, A.B. Gaspar, M.C. Muñoz, J. Chem. Soc., Dalton Trans. (2005) 2062;
(b) P. Gütlich, H.A. Goodwin (Eds.), Top. Curr. Chem. (2004) 233.
[4] (a) S.-I. Ohkoshi, H. Tokoro, K. Hashimoto, Coord. Chem. Rev. 249 (2005) 1380;
(b) F. Varret, A. Bleuzen, K. Boukheddaden, A. Bousseksou, E. Codjovi, C. Enachescu, A. Goujon, J. Linares, N. Menendez, M. Verdaguer, Pure Appl. Chem. 74 (2002) 2159.
[5] (a) M. Gruselle, C. Train, K. Boubekeur, P. Gredin, N. Ovanesyan, Coord. Chem. Rev. 250 (2006) 2491;
(b) A. Beghidja, G. Rogez, P. Rabu, R. Welter, M. Drillon, J. Mater. Chem. 16 (2006) 2715;
(c) K. Inoue, S.-I. Ohkoshi, H. Imai, in: Ref. [1b], vol. 5, ch. 2.
[6] (a) R. Winpenny (Ed.), Struct. Bonding, 2006, p. 122;
(b) D. Gatteschi, R. Sessoli, Angew. Chem. Int. Ed. 42 (2003) 268;
(c) G. Christou, D. Gatteschi, D.N. Hendrickson, R. Sessoli, MRS Bull. 25 (2000) 66;
(d) A. Caneschi, D. Gatteschi, C. Sangregorio, R. Sessoli, L. Sorace, A. Cornia, M.A. Novak, C. Paulsen, W. Wernsdorfer, J. Magn. Magn. Mater. 200 (1999) 182;
(e) J.M. Clemente-Juan, E. Coronado, Coord. Chem. Rev. 193–195 (1999) 361.
[7] (a) S. Blundell, Magnetism in Condensed Matter, Oxford University Press, Oxford, 2001;
(b) H. Lueken, Magnetochemie, Teubner, Stuttgart, Germany, 1999;
(c) O. Kahn, Molecular Magnetism, Wiley-VCH, Weinheim, Germany, 1993.
[8] M. Verdaguer, G.S. Girolami, in: Ref. [1b], vol. 5, ch. 9.
[9] M. Deumal, J. Cirujeda, J. Veciana, J.J. Novoa, Chem. Eur. J. 5 (1999) 1631.
[10] F.H. Köhler, in: Ref. [1b], vol. 1, ch. 12.
[11] (a) I. Bertini, C. Luchinat, G. Parigi (Eds.), Solution NMR of Paramagnetic Molecules, Elsevier, Amsterdam, 2001;
(b) I. Bertini, C. Luchinat, Coord. Chem. Rev. 150 (1996) 1;
(c) L.J. Berliner, J. Reuben (Eds.), NMR of Paramagnetic Molecules, Plenum Press, New York, 1993;
(d) R.S. Drago, Physical Methods for Chemists, Saunders College Publishing, Ft. Worth, 1992, ch. 12;
(e) G.N. La Mar, W.DeW. Horrocks Jr., R.H. Holm (Eds.), NMR of Paramagnetic Molecules, Academic Press, New York, 1973.
[12] L.P. Kazansky, B.R. McGarvey, Coord. Chem. Rev. 188 (1999) 157.
[13] (a) M.J. Duer, Introduction to Solid-state NMR Spectroscopy, Blackwell, Oxford, 2004;
(b) M.J. Duer (Ed.), Solid State NMR Spectroscopy: Principles and Applications, Oxford, 2002;
(c) J.H. Fritzgerald, ACS Symposium Series, vol. 717, 1999;
(d) I. Ando, A.J. Barnes (Eds.), J. Mol. Struct. 335 (1995).
[14] (a) J. Schweizer, E. Ressouche, in: Ref. [1b], vol. 1, ch. 10.;
(b) B. Grillon, in: Ref. [1b], ch. 11.
[15] (a) Ref. [1c], ch. 3.2.;
(b) P. Turek, in: Ref. [1d], ch. 24.
[16] C. Cartier dit Moulin, B. Gillon, F.H. Köhler, R. Lescouëzec, M. Verdaguer, in preparation.
[17] M. Kaupp, M. Bühl, V.G. Malkin, Calculation of NMR and EPR Parameters: Theory and Applications, Wiley-VCH, Weinheim, 2004.
[18] See, e.g.:
(a) S.J. Wilkens, B. Xia, F. Weinhold, J.L. Markley, W.M. Westler, J. Am. Chem. Soc. 120 (1998) 4806;
(b) S.J. Wilkens, B. Xia, B.F. Volkman, F. Weinhold, J.L. Markley, W.M. Westler, J. Phys. Chem. B 102 (1998) 8300;
(c) T.E. Machonkin, W.M. Westler, J.L. Markley, Inorg. Chem. 44 (2005) 779.
[19] (a) J. Mao, Y. Zhang, E. Oldfield, J. Am. Chem. Soc. 124 (2002) 13911;
(b) Y. Zhang, E. Oldfield, J. Am. Chem. Soc. 130 (2008) 3814.
[20] Y. Zhang, H. Sun, E. Oldfield, J. Am. Chem. Soc. 127 (2005) 3652.
[21] Z. Rinkevicius, J. Vaara, L. Telyatnyk, O. Vahtras, J. Chem. Phys. 118 (2003) 2550.
[22] S. Moon. S. Patchkovskii, in: Ref. [17], ch. 20, p. 325.
[23] T.O. Pennanen, J. Vaara, J. Chem. Phys. 123 (2005) 174102.
[24] P. Hrobárik, R. Reviakine, A.V. Arbuznikov, O.L. Malkina, V.G. Malkin, F.H. Köhler, M. Kaupp, J. Chem. Phys. 126 (2007) 024107.
[25] T.O. Pennanen, J. Vaara, Phys. Rev. Lett. 100 (2008) 133002.
[26] (a) L. Helm, Prog. NMR Spectrosc. 49 (2006) 45;
(b) J. Kowalewski, D. Kruk, G. Parigi, Adv. Inorg. Chem. 57 (2005) 41;
(c) L. Banci, in: Ref. [11c], ch. 2.
[27] R.J. Kurland, B.R. McGarvey, J. Magn. Reson. 2 (1970) 286.
[28] (a) I. Bertini, C. Luchinat, G. Parigi, Eur. J. Inorg. Chem. (2000) 2473;
(b) B.R. McGarvey, Inorg. Chem. 34 (1995) 6000;
(c) H. Eicher, Chem. Phys. 86 (1984) 331, and 95 (1985) 341;
(d) H. Eicher, Z. Naturforsch. A 41 (1986) 715.
[29] F. Keffer, T. Oguchi, W. O'Sullivan, J. Yamashita, Phys. Rev. 115 (1959) 1553.
[30] M.L. Munzarová, in: Ref. [17], ch. 29, p. 463.
[31] M.L. Munzarová, P. Kubáček, M. Kaupp, J. Am. Chem. Soc. 112 (2000) 11900.
[32] (a) H.M. McConnell, J. Chem. Phys. 24 (1956) 764;
(b) M. Karplus, G.K. Fraenkel, J. Chem. Phys. 35 (1961) 1312;
(c) T. Yonezawa, T. Kawamura, H. Kato, J. Chem. Phys. 59 (1969) 3482.
[33] H. Eicher, F.H. Köhler, Chem. Phys. 128 (1988) 297.
[34] H. Heise, F.H. Köhler, M. Herker, W. Hiller, J. Am. Chem. Soc. 124 (2002) 10823.
[35] S. Altmannshofer, E. Herdtweck, F.H. Köhler, R. Miller, R. Mölle, E.-W. Scheidt, W. Scherer, C. Train, Chem. Eur. J. 14 (2008) 8013.
[36] A.J. Vega, D. Fiat, Pure Appl. Chem. 32 (1972) 307.
[37] H.M. McConnel, R.E. Robertson, J. Chem. Phys. 29 (1958) 1361.
[38] (a) M. Mehring, Principles of High Resolution NMR in Solids, Springer, Berlin, 1983;
(b) U. Haeberlen, High Resolution NMR in Solids, Academic Press, New York, 1976.
[39] (a) H. Eicher, F.H. Köhler, R.-D. Cao, J. Chem. Phys. 86 (1987) 1829;
(b) R.M. Golding, R.O. Pascual, J. Vrbancich, Mol. Phys. 31 (1976) 731.
[40] A. Nayeem, J.P. Yesinowski, J. Chem. Phys. 89 (1988) 4600.
[41] H. Heise, F.H. Köhler, X. Xie, J. Magn. Reson. 150 (2001) 198.
[42] (a) J. Vaara, O.L. Malkina, H. Stoll, V.G. Malkin, M. Kaupp, J. Chem. Phys. 114 (2001) 61;
(b) O.L. Malkina, B. Schimmelpfennig, M. Kaupp, B.A. Hess, P. Chandra, U. Wahlgren, V.G. Malkin, Chem. Phys. Lett. 296 (1998) 93.
[43] See, e.g.:
(a) Kaupp, in: P. Schwerdtfeger (Ed.), Relativistic Electronic Structure Theory II: Applications, Elsevier, Amsterdam, 2004, ch. 9;
(b) M. Kaupp, O.L. Malkina, V.G. Malkin, P. Pyykkö, Chem. Eur. J. 4 (1998) 118.
[44] F. Neese, J. Chem. Phys. 127 (2007) 164112.
[45] (a) O.L. Malkina, J. Vaara, B. Schimmelpfennig, M.L. Munzarová, V.G. Malkin, M. Kaupp, J. Am. Chem. Soc. 122 (2000) 9206;
(b) M. Kaupp, R. Reviakine, O.L. Malkina, A. Arbuznikov, B. Schimmelpfennig, V.G. Malkin, J. Comput. Chem. 23 (2002) 794;
(c) F. Neese, J. Chem. Phys. 115 (2001) 11080;
(d) F. Neese, J. Chem. Phys. 122 (2005) 034107.
[46] See, e.g.:
(a) F. Neese, J. Chem. Phys. 118 (2003) 3939;
(b) A.V. Arbuznikov, J. Vaara, M. Kaupp, J. Chem. Phys. 120 (2004) 2127;
(c) C. Remenyi, R. Reviakine, A.V. Arbuznikov, J. Vaara, M. Kaupp, J. Phys. Chem. A 108 (2004) 5026.
[47] See, e.g.:
(a) R. Ditchfield, Mol. Phys. 27 (1974) 789;
(b) K. Wolinski, J.F. Hinton, P. Pulay, J. Am. Chem. Soc. 112 (1990) 8251.
[48] W. Kutzelnigg, U. Fleischer, M. Schindler, in: P. Diehl, E. Fluck, H. Günther, R. Kosfeld, J. Seelig (Eds.), NMR Basic Principles and Progress, vol. 213, Springer Verlag, Berlin/Heidelberg, 1991, p. 165ff.
[49] M. Munzarová, M. Kaupp, J. Phys. Chem. A 103 (1999) 9966.
[50] (a) Ref. [1c], ch. 4.3.;
(b) D.B. Amabilino, J. Veciana, in: Ref. [1b], vol. II, ch. 1.;
(c) K. Awaga, in: Ref. [1d], ch. 23.
[51] (a) P. Rey, V.I. Ovcharenko, in: Ref. [1b], vol. IV, ch. 2.;
(b) D. Gatteschi, P. Rey, in: Ref. [1d], ch. 29.
[52] H. Heise, F.H. Köhler, F. Mota, J.J. Novoa, J. Veciana, J. Am. Chem. Soc. 121 (1999) 9659.
[53] J.F.W. Keana, Chem. Rev. 78 (1978) 37.
[54] (a) C. Stroh, R. Ziessel, G. Raudaschl-Sieber, F.H. Köhler, P. Turek, J. Mater. Chem. 15 (2005) 850;

(b) R. Ziessel, C. Stroh, H. Heise, F.H. Köhler, P. Turek, N. Claiser, M. Souhassou, C. Lecompte, J. Am. Chem. Soc. 126 (2004) 12604;
(c) C. Rancurel, H. Heise, F.H. Köhler, U. Schatzschneider, E. Rentschler, J. Vidal-Gancedo, J. Veciana, J.-P. Sutter, J. Phys. Chem. A 108 (2004) 5903;
(d) C. Sporer, H. Heise, K. Wurst, D. Ruiz-Molina, H. Kopacka, P. Jaitner, F. Köhler, J.J. Novoa, J. Veciana, Chem. Eur. J. 10 (2004) 1355;
(e) G. Maruta, S. Takeda, A. Yamaguchi, T. Ohuno, K. Awaga, Polyhedron 22 (2003) 1989;
(f) G. Maruta, S. Takeda, A. Yamaguchi, T. Ohuno, K. Awaga, K. Yamaguchi, Mol. Cryst. Liq. Cryst. 334 (1999) 295.
[55] L. Telyatnyk, J. Vaara, Z. Rinkevicius, O. Vahtras, J. Phys. Chem. B 108 (2004) 1197.
[56] M. Jaeggy, F.H. Köhler, unpublished.
[57] A. Zheludev, M. Bonnet, E. Ressouche, J. Schweizer, M. Wan, H. Wang, J. Magn. Magn. Mater. 135 (1994) 147.
[58] J.S. Miller, A.J. Epstein, W.M. Reiff, Acc. Chem. Res. 21 (1988) 114.
[59] (a) G.T. Yee, J.S. Miller, in: Ref. [1b], vol. V, ch. 7.;
(b) V. Gama, M.T. Duarte, in: Ref. [1b], vol. V, ch. 1.
[60] C. Kollmar, O. Kahn, Acc. Chem. Res. 26 (1993) 259.
[61] J. Blümel, N. Hebendanz, P. Hudeczek, F.H. Köhler, W. Strauss, J. Am. Chem. Soc. 114 (1992) 4223.
[62] J. Blümel, M. Herker, W. Hiller, F.H. Köhler, Organometallics 15 (1996) 3474.
[63] (a) F.H. Köhler, K.-H. Doll, W. Prößdorf, Angew. Chem. Int. Ed. Engl. 19 (1980) 479;
(b) N. Hebendanz, F.H. Köhler, G. Müller, J. Riede, J. Am. Chem. Soc. 108 (1986) 3281;
(c) F.H. Köhler, W. Prößdorf, J. Am. Chem. Soc. 100 (1978) 5971;
(d) F.H. Köhler, X. Xie, Magn. Reson. Chem. 35 (1997) 487;
(e) N. Hebendanz, F.H. Köhler, F. Scherbaum, B. Schlesinger, Magn. Reson. Chem. 27 (1989) 798.
[64] T. Pennanen, J. Vaara, Personal communication to M. K.
[65] J. Schweizer, S. Golhen, E. Lelièvre-Berna, L. Quahab, Y. Pontillon, E. Ressouche, Physica B 297 (2001) 213.
[66] M.A. Sheibat, L.B. Casabianca, N.P. Wickramasinghe, S. Guggenheim, A.C. de Dios, Y. Ishii, J. Am. Chem. Soc. 129 (2007) 10968.
[67] D. Carlier, M. Ménétrier, C.P. Grey, C. Delmas, G. Ceder, Phys. Rev. B 67 (2003) 174103.
[68] G. Kervern, G. Pintacuda, Y. Zhang, E. Oldfield, C. Roukoss, E. Kuhn, E. Herdtweck, J.-M. Basset, S. Cadars, A. Lesage, C. Coperet, L. Emsley, J. Am. Chem. Soc. 128 (2006) 13545.
[69] P. Fernández, H. Pritzkow, J.J. Carbó, P. Hofmann, M. Enders, Organometallics 26 (2007) 4402.
[70] S. Kemper, P. Hrobárik, M. Kaupp, N.E. Schlörer, submitted for publication.